Evaluation of the Roller Arrangements for the Ball-Dribbling Mechanisms Adopted by RoboCup Teams

Research Article

Evaluation of the Roller Arrangements for the Ball-Dribbling Mechanisms Adopted by RoboCup Teams

Kenji Kimura[1,*], Shota Chikushi[2], Kazuo Ishii[1]

[1]Graduate School of Life Science and Engineering, Kyusyu Institute of Technology, 2-4 Hibikino, Wakamatsu-ku, Kitakyushu 808-0196, Fukuoka, Japan
[2]Department of Precision Engineering, The University of Tokyo, Hongo 7-3-1, Bunkyo-ku 113-8656, Tokyo, Japan

ARTICLE INFO

ABSTRACT

The middle-size league soccer competition is an important RoboCup event designed to promote advancements in Artificial Intelligence (AI) and robotics. In recent years, soccer robots using a dribbling mechanism, through which the ball is controlled using two driving rollers, have been adopted by teams worldwide. A survey conducted during the 2017 World Cup in Nagoya revealed that the teams determined their roller arrangements heuristically without the use of a formal mathematical process. In this study, we focus on sphere slip speed to develop a mathematical model for sphere rotational motion, allowing for slip. Using this framework, we derived the relationship between the sphere slip and mobile speeds and evaluated the roller arrangements used by the participating teams.

1. INTRODUCTION

RoboCup is an international project that promotes innovation in Artificial Intelligence (AI), robotics, and related domains. It represents an attempt to develop AI and autonomous robotics research by providing a fundamental problem that can be solved by integrating a wide range of technologies. In particular, the middle-size league soccer competition is a RoboCup event providing a dynamical environment in which many robots cooperate with humans within the same space.

Various developments have been made in the RoboCup middle-size league soccer robot [1,2]. These robots generally have a mechanism similar to that of an omnidirectional movement mechanism using three-omni wheels [3] or that using four-omni wheels [4] and so on, and in recent years, this mechanism is involved in controlling the rotation of a ball. The ball holding mechanism is used.

In the past, several teams have equipped their robots such as arm type [5,6], bar type [7,8] and single-wheel type [9] with ball dribbling mechanisms for controlling the rotation of the ball. To be useful in soccer play, the dribbling performance of such mechanisms must be skillful. However, they cannot grasp a ball and control. Recently, dribbling devices use rollers to grasp the upper half of the ball to enable them to maintain a pull on it while driving in reverse. Friction is generated between the ball and rollers by a spring mounted on a supporting lever. To maintain dribbling, it is essential that the roller and ball rotate with approximately the same speed and that the ball moves in the same direction as the robot. Many robots, such as that deployed by the Turtles team [10], rely on ball handling force and use a roller arrangement in which there is slip between the roller and ball. To determine their roller arrangement, the Turtles rely on heuristic measures and experimental results. Although slip causes loss of speed in a moving sphere, the resulting friction can improve the ball holding power and rotational stability. Accordingly, slip is an important factor.

The authors conducted an investigation of the ball dribbling mechanisms employed by the teams at the 2017 middle-size league soccer competition in Nagoya, Japan. Table 1 lists our survey results, including team name and roller type, shape, and arrangement angle. The four shapes [□○△◇] in the "Symbol" column indicate the roller angles used by the respective teams. Figure 1 shows the rotational axis, ball velocity, and roller velocity in reverse motion of a dual-roller arrangement. The RV-Infinity [11] roller arrangement in Table 1 involves no slip (see Figure 1a) because the roller velocity corresponds to the ball velocity; i.e., the rollers' rotational axes are aligned on a plane that includes the origin of the ball's sphere [12,13]. In another approach, CAMBADA [14] avoids slippage through the use of unconstrained rollers (omni-rollers).

Other teams, namely the Turtles [10], Falcons, Musashi150 [15], NuBot [16], and Water, have adopted roller arrangements that allow for slip to occur (see Figure 1b) through a differential between roller and ball velocity. Based on analysis of sphere rotational motion in which slip is allowed, we developed a sphere kinematics model in which dual-constraint rollers allow for slipping [17].

In this study, we validated the model introduced in Kimura et al. [17] and evaluated the roller arrangements used by the competition teams from the standpoint of sphere speed, efficiency, and sphere slip speed (ball-holding power).

Corresponding author. Email: kimuken1977_2058@yahoo.co.jp

Table 1 | Survey result of roller type and angle in world teams

Team name	Symbol	Roller type	Angle
RV-infinity [11]	□ R	Constraint	0°
The Turtles [10]	○ T	Constraint	10°
Falcons	○ F	Constraint	10°
Musashi150 [15]	△ H	Constraint	20°
NuBot [16]	△ N	Constraint	20°
Water	◇ W	Constraint	30°
CAMBADA	–	Unconstraint	50°
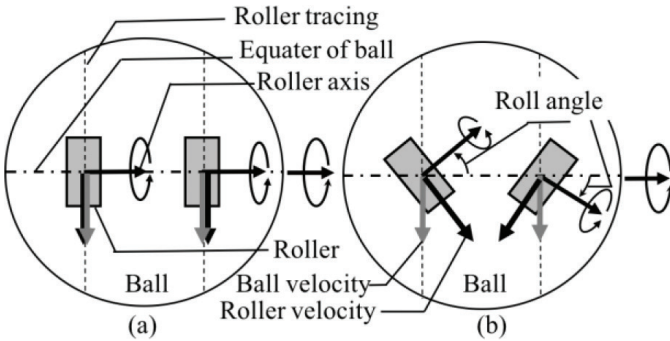
Figure 1 | The ball reverse motion by two-rollers arrangement in the ball-dribbling mechanism. Case of (a) is zero-roller angle and case of (b) is non-zero-roller angle.

The remainder of this paper is organized as follows. In Section 2, we introduce a sphere kinematics model that allows for slipping. In Section 3, we validated the model introduced in Kimura et al. [17] and theoretical formula of sphere slip velocity vector. In Section 4, we considered the distribution of slip velocity vector and the roller arrangement of a ball dribbling mechanism based on the results of a robotic experiment. Finally, in Section 5, we present a summary and discuss future research.

2. THE SLIP VELOCITY VECTOR OF THE SPHERE

We quantify the slip between the sphere and roller.

As shown in Figure 2a, the center O of a sphere with radius r is fixed as the origin of the coordinate system $\Sigma - xyz$. The i-th constraint roller is in point contact with the sphere at a position vector P_i and is arranged such that the center of mass of the roller P_C, P_i and O are on the same line. $\boldsymbol{\omega}$ denotes the angular velocity vector of the sphere. $\boldsymbol{\eta}_i$ denotes the unit vector along the rotational axis of constraint roller. v_i the denotes peripheral speed of the constraint roller. α_i $(-90° \leq \alpha_i \leq 90°)$ denotes roller arrangement angle between $\boldsymbol{\eta}_i$ and $\mathbf{span}\{P_1, P_2\}$ which has unit normal vector $\boldsymbol{e}$. The great circle C_G passes thorough P_1 and P_2 are on the sphere. Normal orthogonal base $\{X_i, e\}$ exist on the tangent plane $\mathbf{span}\{X_i, e\}$ at the P_i (see Figure 2b and 2c). $\mathcal{V}_i^S$ and $\mathcal{V}_i^R$ are sphere's rotational speed and roller's rotational speed at P_i, respectively. The slip velocity of sphere $\boldsymbol{\zeta}_i$ can be represented as difference between $\mathcal{V}_i^S$ and $\mathcal{V}_i^R$. $\boldsymbol{\zeta}_i$ can be represented as $S_i X_i + T_i e$ (linear combination of X_i and e) and the coefficients S_i and T_i can be represented as Equations (1)–(3).

$$S_i = \langle \boldsymbol{\zeta}_i, X_i \rangle \tag{1}$$

$$T_i = \langle \boldsymbol{\zeta}_i, \boldsymbol{e} \rangle = 0 \quad \text{(for all } v_1, v_2) \tag{2}$$

where,

$$\boldsymbol{\zeta}_i = \mathcal{V}_i^S - \mathcal{V}_i^R = \boldsymbol{\omega} \times P_i - v_i e_i \tag{3}$$

3. VERIFICATION OF THEORETICAL FORMULA

In this chapter, we verified theoretical formulas including sphere kinematic (Section 3.1) and sphere slip velocity vector (Section 3.2) in reverse motion.

As shown in Figure 3, the conditions are given as follows: $\theta_{1,1} = 215°$, $\theta_{1,2} = 325°$, $\theta_{1,2}$, $\theta_{2,2} = 60°$, $r = 0.1$ (m), $\alpha_1 = \alpha$, $\alpha_2 = -\alpha$ (symmetry roller arrangement). Five experiments were conducted, each at the same four different degrees angles ($\alpha = 0°, 10°, 20°, 30°$).

3.1. Verification of Kinematics

As shown in Table 2, $\|V\|$, φ and ρ are values calculated from v_1, $v_2 = -0.91$ (m/s) by Equations (11) and (14) refer to Kimura et al. [17]. v_1^m, v_2^m are theoretical values (controlled values which have target values v_1, $v_2 = -0.91$ (m/s)). $\|V\|_m$, φ_m and ρ_m are theoretical values calculated from v_1^m, v_2^m by Equations (11) and (14) refer to Kimura et al. [17]. $\|V\|_e$, φ_e and ρ_e are experimental values measured from
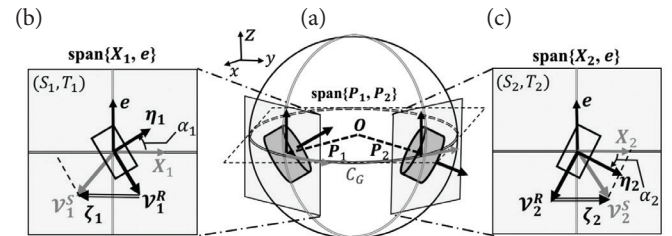
Figure 2 | The existence of sphere slip velocity vector. (a) Isometric view. (b) Left side roller on $\mathbf{span}\{X_1, e\}$. (c) Right side roller on $\mathbf{span}\{X_2, e\}$.
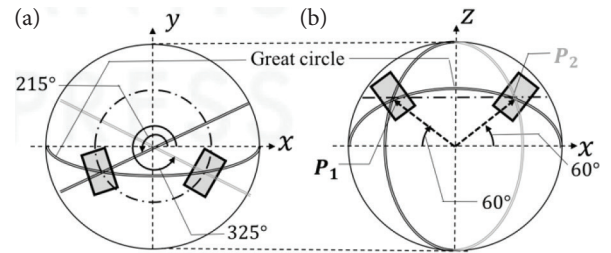
Figure 3 | The location of contacted rollers on sphere for experiment. (a) Top view. (b) Back view.

Table 2 | Values calculated from v_1, $v_2 = -0.91$ (m/s)

α	0°	10°	20°	30°
$\|V\|$ (m/s)	1	0.98	0.93	0.84
φ (°)	−90	−90	−90	−90
ρ (°)	0	0	0	0

encoder. v_1^e, v_2^e are experimental values calculated from $\|V\|_e$, φ_e and ρ_e by Equation (22) refer to Kimura et al. [17].

3.1.1. Inverse kinematics

Figures 4–7 exhibit the theoretical data v_1^m, v_2^m and experimental data v_1^e, v_2^e. And, Tables 3–6 show the absolute mean error calculated in interval of 7–8 (s). We consider comparison between v_1^m, v_2^m and v_1^e, v_2^e in detail, see below.

In the evaluation case of $\alpha = 0°$, v_1^e and v_2^e are close to v_1^m and v_2^m, respectively (see Figure 4). As shown in Table 3, $\left|v_1^m - v_1^e\right|$ is almost 0.04 (m/s), $\left|v_2^m - v_2^e\right|$ is 0.04 (m/s).
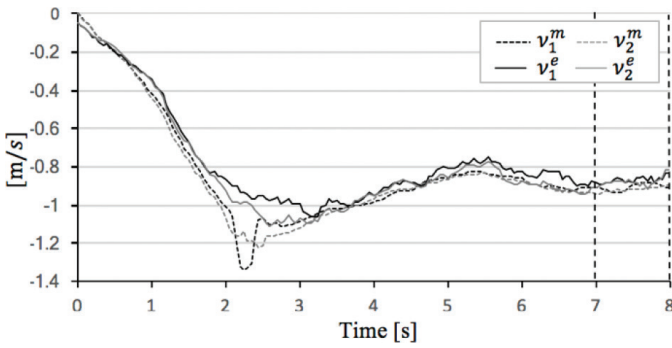
Figure 4 | Comparison theoretical value v_1^m and experimental value in $\alpha = 0°$.
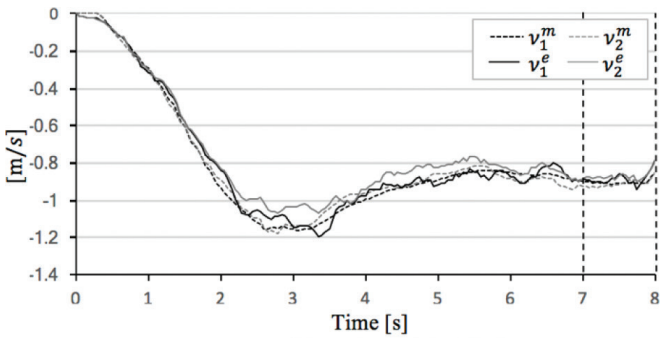
Figure 5 | Comparison theoretical value and experimental value in $\alpha = 10°$.
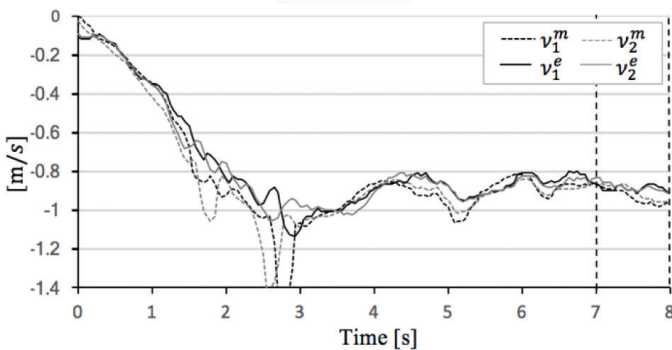
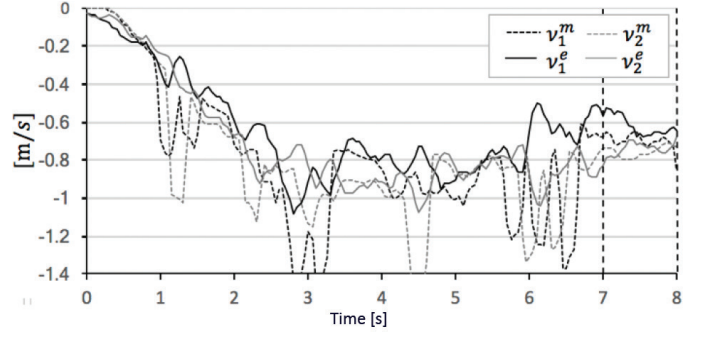**Figure 6** | Comparison theoretical value and experimental value in $\alpha = 20°$.

Figure 7 | Comparison theoretical value and experimental value in $\alpha = 30°$.

Table 3 | Absolute mean error [7–8 (s)] in $\alpha = 0°$

	1	2	3	4	5
$\left|v_1^m - v_1^e\right|$ (m/s)	0.03	0.04	0.10	0.10	0.03
$\left|v_2^m - v_2^e\right|$ (m/s)	0.03	0.04	0.02	0.04	0.04

Table 4 | Absolute mean error [7–8 (s)] case of $\alpha = 10°$

	1	2	3	4	5
$\left|v_1^m - v_1^e\right|$ (m/s)	0.04	0.03	0.08	0.03	0.02
$\left|v_2^m - v_2^e\right|$ (m/s)	0.03	0.04	0.01	0.04	0.04

Table 5 | Absolute mean error [7–8 (s)] case of $\alpha = 20°$

	1	2	3	4	5
$\left|v_1^m - v_1^e\right|$ (m/s)	0.05	0.05	0.06	0.09	0.07
$\left|v_2^m - v_2^e\right|$ (m/s)	0.03	0.03	0.05	0.06	0.05

Table 6 | Absolute mean error [7–8 (s)] case of $\alpha = 30°$

	1
$\left|v_1^m - v_1^e\right|$ (m/s)	0.08
$\left|v_2^m - v_2^e\right|$ (m/s)	0.05

In the evaluation case of $\alpha = 10°$, v_1^e and v_2^e are close to v_1^m and v_2^m, respectively (see Figure 5). As shown in Table 4, $\left|v_1^m - v_1^e\right|$ is almost 0.04 (m/s), $\left|v_2^m - v_2^e\right|$ is 0.04 (m/s).

In the evaluation case of $\alpha = 20°$, v_1^e and v_2^e are close to v_1^m and v_2^m, respectively (see Figure 6). As shown in Table 5, $\left|v_1^m - v_1^e\right|$ is 0.09 (m/s), $\left|v_2^m - v_2^e\right|$ is 0.06 (m/s).

In the evaluation case of $\alpha = 30°$, the limitations of the motor drivers and intense dynamical friction that caused heat between the roller surfaces and the sphere obliged us to cease the second and subsequent experiments. However, $\|V\|_e$, φ_e and ρ_e are partially close to $\|V\|_m$, φ_m and ρ_m, respectively (see Figure 7). And, $\left|v_1^m - v_1^e\right|$ is 0.08 (m/s), $\left|v_2^m - v_2^e\right|$ is 0.05 (m/s) (see Table 6).

Thus, inverse kinematics is validated.

3.1.2. Forward kinematics

Figures 8–11 exhibit the theoretical data $\|V\|_m, \varphi_m, \rho_m$ and experimental data $\|V\|_e, \varphi_e, \rho_e$. And, Tables 7–10 show the absolute mean error calculated in interval of 7–8 (s). We consider comparison between $\|V\|_m, \varphi_m, \rho_m$ and $\|V\|_e, \varphi_e, \rho_e$, respectively in detail, see below.
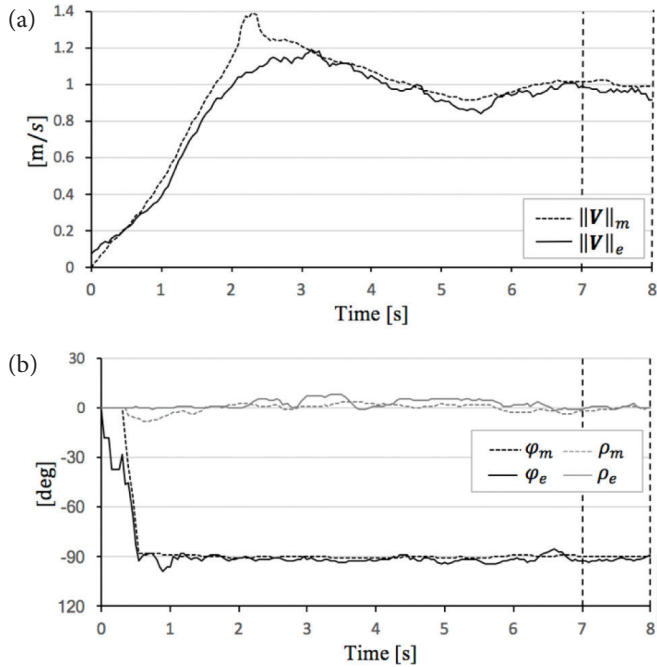
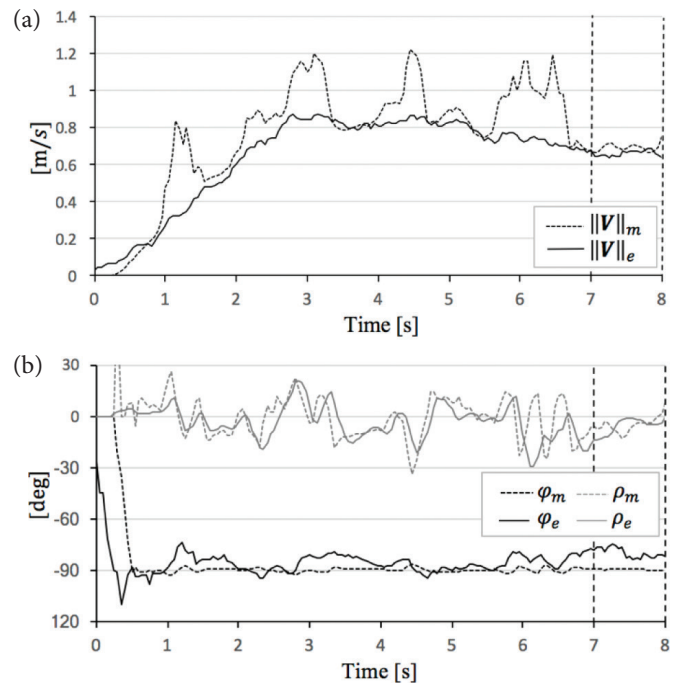**Figure 8** | Comparison theoretical value and experimental value in $\alpha = 0°$. (a) Sphere mobile speed. (b) Sphere direction and angle of sphere rotational axis.
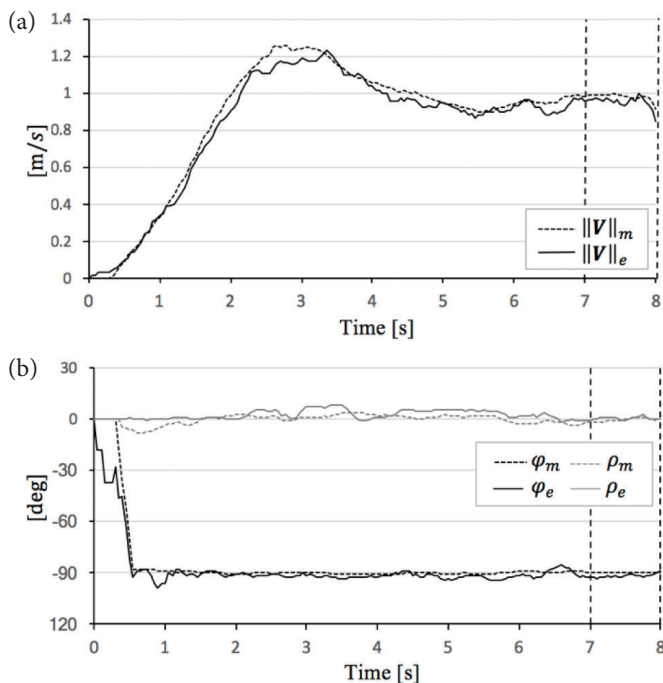
Figure 9 | Comparison theoretical value and experimental value in $\alpha = 10°$. (a) Sphere mobile speed. (b) Sphere direction and angle of sphere rotational axis.
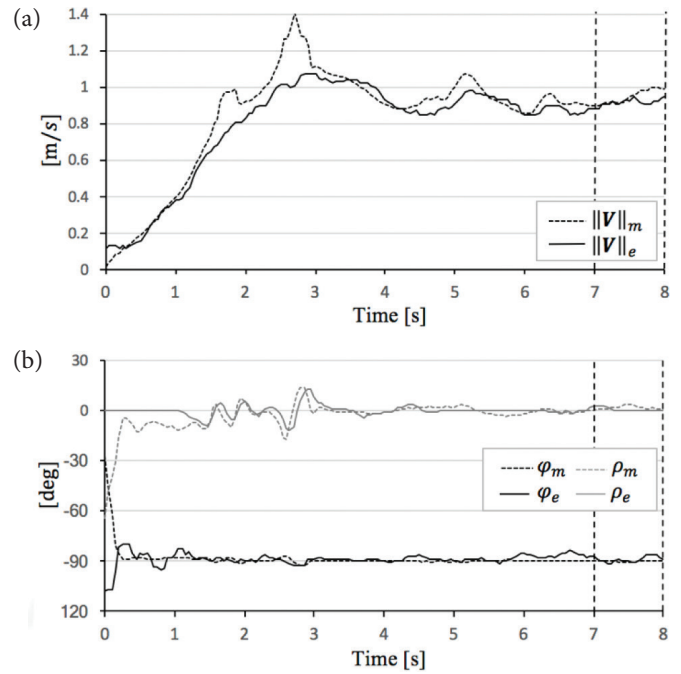
Figure 10 | Comparison theoretical value and experimental value in $\alpha = 20°$. (a) Sphere mobile speed. (b) Sphere direction and angle of sphere rotational axis.

Figure 11 | Comparison theoretical value and experimental value in $\alpha = 30°$. (a) Sphere mobile speed. (b) Sphere direction and angle of sphere rotational axis.

In the evaluation case of $\alpha = 0°$, $\|V\|_e, \varphi_e$ and ρ_e are close to $\|V\|_m$, φ_m and ρ_m, respectively (see Figure 8). As shown in Table 7, $\|\|V\|_m - \|V\|_e\|$ is 0.06 (m/s), $|\varphi_m - \varphi_e|$ is 3.9 (°), and $|\rho_m - \rho_e|$ is 6.3 (°).

In the evaluation case of $\alpha = 10°$, $\|V\|_e, \varphi_e$ and ρ_e are close to $\|V\|_m$, φ_m and ρ_m (see Figure 9). As shown in Table 8, $\|\|V\|_m - \|V\|_e\|$ is 0.04 (m/s), $|\varphi_m - \varphi_e|$ is 3.1 (°), and $|\rho_m - \rho_e|$ is 3.9 (°).

Table 7 | Absolute mean error [7–8 (s)] in $\alpha = 0°$

	1	2	3	4	5
$\| \|V\| \|_m - \| \|V\| \|_e$ (m/s)	0.03	0.04	0.05	0.06	0.04
$\|\varphi_m - \varphi_e\|$ (°)	1.5	1.6	2.2	3.9	0.8
$\|\rho_m - \rho_e\|$ (°)	0.7	0.9	6.3	5.3	0.9

Table 8 | Absolute mean error [7–8 (s)] in $\alpha = 10°$

	1	2	3	4	5
$\| \|V\| \|_m - \| \|V\| \|_e$ (m/s)	0.03	0.04	0.04	0.03	0.03
$\|\varphi_m - \varphi_e\|$ (°)	1.2	1.8	3.1	2.2	2.0
$\|\rho_m - \rho_e\|$ (°)	2.1	1.0	3.9	1.2	1.2

Table 9 | Absolute mean error [7–8 (s)] in $\alpha = 20°$

	1	2	3	4	5
$\| \|V\| \|_m - \| \|V\| \|_e$ (m/s)	0.03	0.03	0.06	0.07	0.05
$\|\varphi_m - \varphi_e\|$ (°)	1.5	2.3	2.7	2.7	4.3
$\|\rho_m - \rho_e\|$ (°)	1.9	1.4	2.1	2.1	2.1

Table 10 | Absolute mean error [7–8 (s)] in $\alpha = 30°$

	1
$\| \|V\| \|_m - \| \|V\| \|_e$ (m/s)	0.04
$\|\varphi_m - \varphi_e\|$ (°)	9.7
$\|\rho_m - \rho_e\|$ (°)	5.1

Table 11 | Values calculated from $v_1, v_2 = -0.91$ (m/s)

α	0°	10°	20°	30°
S_1 (m/s)	0	−0.16	−0.31	−0.45
T_1 (m/s)	0	0	0	0
S_2 (m/s)	0	0.16	0.31	0.45
T_2 (m/s)	0	0	0	0

In the evaluation case of $\alpha = 20°$, $\| \|V\| \|_e$, φ_e and ρ_e are close to $\| \|V\| \|_m$, φ_m and ρ_m, respectively (see Figure 10). As shown in Table 9, $\| \|V\| \|_m - \| \|V\| \|_e$ is 0.07 (m/s), $\|\varphi_m - \varphi_e\|$ is 4.3 (°), and $\|\rho_m - \rho_e\|$ is 2.1 (°).

In the evaluation case of $\alpha = 30°$, the data have intense behavior due to limitations of the motor drivers. However, $\| \|V\| \|_e$, φ_e and ρ_e are partially close to $\| \|V\| \|_m$, φ_m and ρ_m, respectively (see Figure 11). And, $\| \|V\| \|_m - \| \|V\| \|_e$ is 0.04 (m/s), $\|\varphi_m - \varphi_e\|$ is 9.7 (°), and $\|\rho_m - \rho_e\|$ is 5.1 (°) (see Table 10).

Thus, forward kinematics is validated.

## 3.2. Consideration of Slip Velocity Vector

As shown in Table 11, S_i ($i = 1, 2$) are values calculated from $v_1, v_2 = -0.91$ (m/s) by Equation (1). S_i^m ($i = 1, 2$) are theoretical values calculated from v_1^m and v_2^m by Equation (1). S_i^e and T_i^e ($i = 1, 2$) are experimental values calculated from $\| \|V\| \|_e$, φ_e, ρ_e, v_1^e and v_2^e by Equations (1) and (2).

Using Equation (2) as $v_i = v_i^m$ ($i = 1, 2$), we give $T_i^m = 0$ ($i = 1, 2$). And, as $v_i = v_i^e$ ($i = 1, 2$), we give $T_i^e = 0$ ($i = 1, 2$). Thus, $\left\| T_i^m \right\| - \left| T_i^e \right\| = 0$ and, ζ_1 and ζ_2 are correspond to tangent vectors on a great circle C_G.

Figures 12–15 exhibit the theoretical data S_i^m ($i = 1, 2$) and experimental data S_i^e ($i = 1, 2$). And, Tables 12–15 show the absolute mean error [calculated in interval of 7–8 (s)]. We consider comparison between S_i^m ($i = 1, 2$) and S_i^e ($i = 1, 2$) in detail, see below.
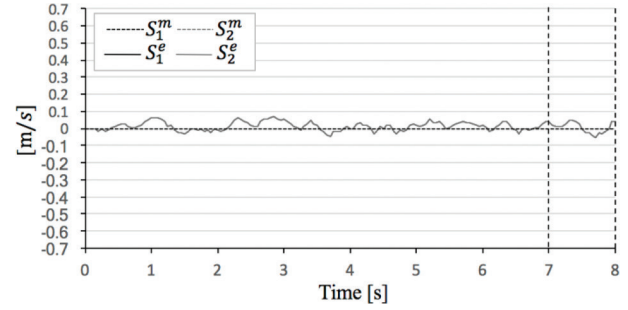
Figure 12 | Comparison theoretical value and experimental value in $\alpha = 0°$.
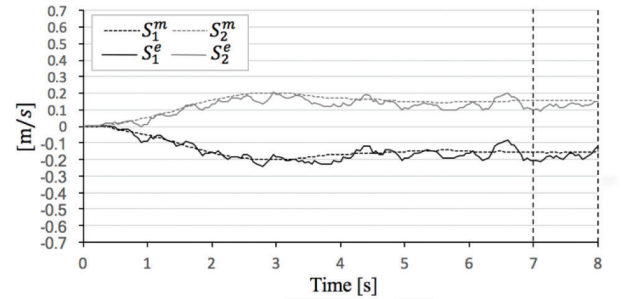
Figure 13 | Comparison theoretical value and experimental value in $\alpha = 10°$.
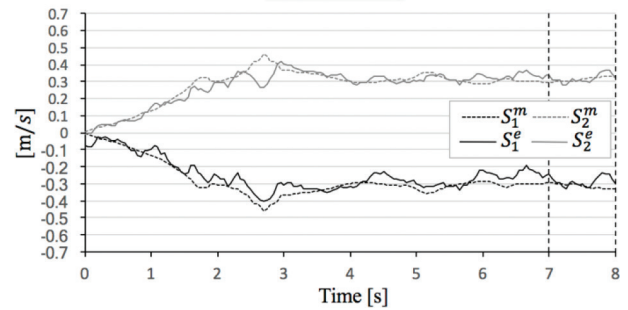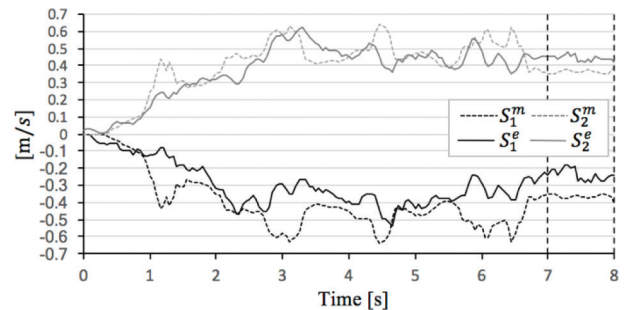

Figure 14 | Comparison theoretical value and experimental value in $\alpha = 20°$.

Figure 15 | Comparison theoretical value and experimental value in $\alpha = 30°$.

In the evaluation case of $\alpha = 0°$, S_1^e and S_2^e are close to S_1^m and S_2^m, respectively (see Figure 12). As shown in Table 12, $\left\|S_1^m\right| - \left|S_1^e\right\|$ is 0.04 (m/s) and $\left\|S_2^m\right| - \left|S_2^e\right\|$ is 0.04 (m/s).

In the evaluation case of $\alpha = 10°$, S_1^e and S_2^e are close to S_1^m and S_2^m, respectively (see Figure 13). As shown in Table 13, $\left\|S_1^m\right| - \left|S_1^e\right\|$ is 0.04 (m/s) and $\left\|S_2^m\right| - \left|S_2^e\right\|$ is 0.04 (m/s).

In the evaluation case of $\alpha = 20°$, S_1^e and S_2^e are close to S_1^m and S_2^m, respectively (see Figure 14). As shown in Table 14, $\left\|S_1^m\right| - \left|S_1^e\right\|$ is 0.09 (m/s) and $\left\|S_2^m\right| - \left|S_2^e\right\|$ is 0.05 (m/s).

In the evaluation case of $\alpha = 30°$, the data have intense behavior due to limitations of the motor drivers. However, S_1^e and S_2^e are partially close to S_1^m and S_2^m, respectively (see Figure 15). And, $\left\|S_1^m\right| - \left|S_1^e\right\|$ is 0.13 (m/s) and $\left\|S_2^m\right| - \left|S_2^e\right\|$ is 0.08 (m/s) (see Table 15).

Thus, Equations (1)–(3) is validated by experiment.

Table 12 | Absolute mean error [7–8 (s)] in $\alpha = 0°$

	1	2	3	4	5
$\left|S_1^m - S_1^e\right|$ (m/s)	0.02	0.03	0.02	0.04	0.01
$\left|S_2^m - S_2^e\right|$ (m/s)	0.02	0.03	0.02	0.04	0.01

Table 13 | Absolute mean error [7–8 (s)] in $\alpha = 10°$

	1	2	3	4	5
$\left|S_1^m - S_1^e\right|$ (m/s)	0.02	0.03	0.04	0.03	0.03
$\left|S_2^m - S_2^e\right|$ (m/s)	0.02	0.03	0.03	0.04	0.03

Table 14 | Absolute mean error [7–8 (s)] in $\alpha = 20°$

	1	2	3	4	5
$\left|S_1^m - S_1^e\right|$ (m/s)	0.03	0.04	0.06	0.05	0.09
$\left|S_2^m - S_2^e\right|$ (m/s)	0.02	0.03	0.02	0.03	0.05

Table 15 | Absolute mean error [7–8 (s)] in $\alpha = 30°$

	1
$\left|S_1^m - S_1^e\right|$ (m/s)	0.13
$\left|S_2^m - S_2^e\right|$ (m/s)	0.08

4. CONSIDERATION OF WORLD TEAMS' ROLLERS ARRANGEMENT

Figure 16 shows the relationship between the sphere slip speed and sphere mobile speed. The horizontal and vertical axes show S_i^e ($i = 1, 2$) and $\|V\|_e$, respectively.

The configurations [■●▲◆] (left-side roller) and [■●▲◆] (right-side roller) indicate the coordinates $[S_1^e, \|V\|_e]^T$ and $[S_2^e, \|V\|_e]^T$, respectively, corresponding to the experimental mean values calculated over intervals of 7–8 (s).

4.1. Vertical Coordinate (Mobile Speed)

For [■■] and [●●], the sphere mobile speeds $\|V\|_e$ are closely distributed within a range from 0.89 to 0.98 (m/s). The corresponding distributions of $\|V\|_e$ for [▲▲] are within the ranges from 0.86 to 0.92 (m/s) and [◆◆] are 0.66 (m/s). Thus, [■■] and [●●] have the highest spherical speed efficiencies.

4.2. Horizontal Coordinate (Sphere Slip Speed)

For [■■], the values of $\left|S_1^e\right|$ and $\left|S_2^e\right|$ are generally distributed within the range from 0.01 to 0.03 (m/s). The corresponding distributions of $\left|S_1^e\right|$ and $\left|S_2^e\right|$ for [●●], [▲▲], and [◆◆] are mostly within the ranges from 0.13 to 0.18 (m/s), 0.23 to 0.34 (m/s), and 0.24 to 0.45 (m/s), respectively.

Under this kinematics model, it assumed that the roller and sphere contact at a single point. In reality, of course, they would contact along a surface, causing, ζ_i to generate a frictional force F_i in opposition to ζ_i. Referring to consideration, in which ζ_1 and ζ_2 are aligned back-to-back along a great circle, the frictional forces F_1 and F_2 generated by ζ_1 and ζ_2, respectively, would be in and are opposite directions and face-to-face (from Section 3 refer to Kimura et al. [17]).

For [▲▲] and [◆◆], there is an above-moderate frictional force. The [■■] and [●●] configurations adopted by RV-infinity, the Turtles, and the Falcons have the highest sphere speed efficiencies. However, [■■], the RV-infinity roller configuration, has nearly no friction [$\left|S_1^e\right|$ and $\left|S_2^e\right|$ are close to 0 (m/s)]. By contrast, the configuration [●●] adopted by the Turtles and
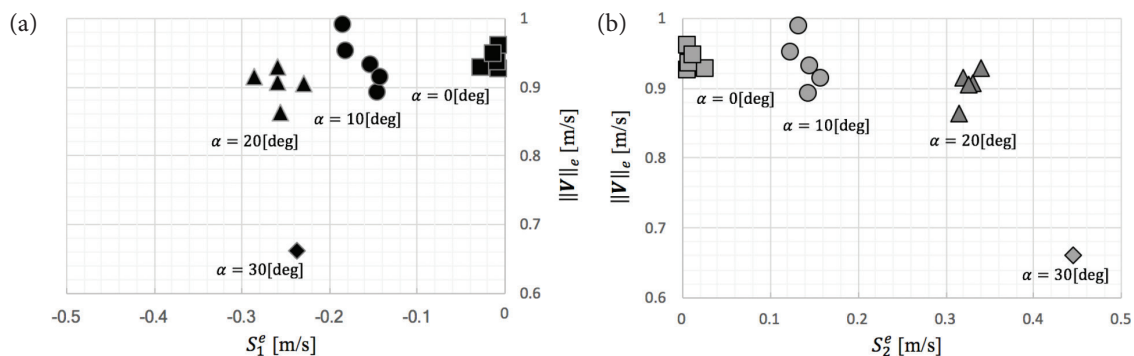
Figure 16 | Relationship between sphere slip speed and sphere mobile speed. (a) Left-side roller. (b) Right-side roller.

Falcons has moderate friction $[\left|S_1^e\right|$ and $\left|S_2^e\right|$ closely distributed within a range from 0.13 to 0.18 (m/s)].

Thus, by adopting [● ●], the Turtles and Falcons have developed roller systems with the optimum arrangement at $\alpha = 10°$.

5. CONCLUSION

In this study, we verified derive the sphere kinematics that allows for slipping and considered sphere slip velocity vector and evaluated the roller arrangement used by the world teams. As a result, Tech United Turtles and Falcons have adopted optimum roller arrangement in teams of mobile speed efficiency.

In future studies, by applying the ball-dribbling mechanism, this model should be verified experimentally.

CONFLICTS OF INTEREST

The authors declare they have no conflicts of interest.

REFERENCES

[1] R.J.G. Alaerds, Mechanical design of the next generation Tech United Turtle, Technische Universiteit Eindhoven, 2010.

[2] Y. Takemura, Y. Ogawa, A.A.F. Nassiraei, A. Sanada, Y. Kitazumi, I. Godler, et al., A system design concept based on omni-directional mobility, safety and modularity for an autonomous mobile soccer robot, J. Bionic. Eng. 5 (2008), 121–129.

[3] J. Tang, K. Watanabe, K. Kuribayashi, Y. Shiraishi, Autonomous control for an omnidirectional mobile robot with the orthogonal-wheel assembly, J. Robot. Soc. Japan 17 (1999), 51–60.

[4] S. Fujisawa, K. Ohkubo, Y. Shidama, H. Yamaura, Kinematics and moving properties of a four wheel-drive, omnidirectional mobile robot, Japan. Soc. Mech. Eng. 62 (1996), 4573–4579.

[5] K. Fujimoto, K. Ishii, Y. Kitazumi, Development of a ball handling mechanism for a RoboCup Soccer Robot, in: The Robotics and Mechatronics Conference, 2011, pp. 2A2-F08(1)–(4).

[6] J. de Best, R. van de Molengraft, M. Steinbuch, A novel ball handling mechanism for the RoboCup middle size league, Mechatronics 21 (2011), 469–478.

[7] D.G.H. Smit, Robocup small size league: active ball handling system, Stellenbosch University, Master in Engineering (Mechatronic), 2014.

[8] R. D'Andrea, T. Kalmar-Nagy, P. Ganguly, M. Babish, The Cornell RoboCup Team, in: P. Stone, T. Balch, G. Kraetzschmar (Eds.), RoboCup 2000, Robot SoccerWorld Cup IV, Berlin, Heidelberg, Springer, 2001, pp. 41–51.

[9] N. Lau, L.S. Lopes, G.A. Corrente, CAMBADA: information sharing and team coordination, in: Proceedings of the 8th Conference on Autonomous Robot Systems and Competitions, Portuguese Robotics Open - ROBOTICA 2008, Aveiro, Portugal, 2008, pp. 27–32.

[10] K.P. Gerrits, M.J.G. van de Molengraft, R. Hoogendijk, Ball handling system for tech united soccer robots, 2012.

[11] Y. Yasohara, K. Shimizu, H. Suzuki, Development of ball handling mechanism for RoboCup MSL, in: Proceedings of the 30th Fuzzy System Symposium, Kochi, Kerala, India. 2014, pp. 616–617.

[12] K. Kimura, K. Ishii, Y. Takemura, M. Yamamoto, Mathematical modeling and motion analysis of the wheel based ball retaining mechanism, in: 2016 Joint 8th International Conference on Soft Computing and Intelligent Systems (SCIS) and 17th International Symposium on Advanced Intelligent Systems (ISIS), Sapporo, Japan, IEEE, 2016, pp. 518–523.

[13] S. Chikushi, T. Weerakoon, T. Sonoda, K. Ishii, Kinematics of two-roller-driven ball for RoboCup soccer robot, J. Robot. Netw. Artif. Life 4 (2017), 248–253.

[14] R. Dias, A.J.R. Neves, J.L. Azevedo, B. Cunha, J. Cunha, P. Dias, et al., CAMBADA 2013: Team Description Paper, 2013.

[15] S. Chikushi, M. Kuwada, T. Sonoda, A.A.F. Nassiraei, K. Ishii, Development of next-generation soccer robot "Musashi150" for RoboCup MSL, in: Proceedings of the 30th Fuzzy System Symposium, 2014, pp. 624–627.

[16] R. Junkai, X. Chenggang, X. Junhao, H. Kaihong, L. Huimin, A control system for active ball handling in the RoboCup middle size league. in: Chinese Control and Decision Conference (CCDC), Yinchuan, China, IEEE, 2016, pp. 4396–4402.

[17] K. Kimura, K. Ogata, K. Ishii, Novel mathematical modeling and motion analysis of a sphere considering slipping, J. Robot. Netw. Artif. Life 6 (2019), 27–32.

Authors Introduction

Mr. Kenji Kimura

He received the ME (mathematics) from Kyusyu University in 2002. Then he was a mathematical teacher and involved in career guidance in high school up to 2014. Currently, he is an educator of International Baccalaureate Diploma Program (Mathematics: applications and interpretation, analysis and approaches) in Fukuoka Daiichi High School, and student in the doctoral program of the Kyushu Institute of Technology. His current research interests are spherical mobile robot kinematics, control for object manipulation.

Dr. Shota Chikushi
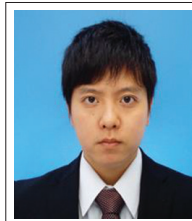
He received the M.S. and D.S. degrees from the Department of Life Science and Systems Engineering, Kyushu Institute of Technology, Fukuoka, Japan, in 2012 and 2018, respectively. He is an Assistant professor in the Department of Precision Engineering, Graduate School of Engineering, University of Tokyo. From 2015 to 2018, he was an Assistant professor of the Nippon Bunri University, Oita, Japan. His research interests are motion control of a roller-driven sphere, design for autonomous omnidirectional mobile robot and operation support of disaster response robot in unmanned construction.

Dr. Kazuo Ishii

He is a Professor in the Kyushu Institute of Technology, where he has been since 1996. He received his PhD degree in Engineering from University of Tokyo, Tokyo, Japan, in 1996. His research interests span both Ship Marine Engineering and Intelligent Mechanics. He holds five patents derived from his research. His lab got "Robo Cup 2011 Middle Size League Technical Challenge 1st Place" in 2011. He is a member of the Institute of Electrical and Electronics Engineers, the Japan Society of Mechanical Engineers, Robotics Society of Japan, the Society of Instrument and Control Engineers and so on.